Pullout Capacity of Single and Biwing Anchors in a Soft Clay Deposit
Model Investigation in a Centrifuge and FEM Predictions

Fanning, J.; Sivakumar, V.; Nanda, S.; Gavin, K.; Murray, T.; Bradshaw, A.; Black, J.; Jalilvand, S.

DOI
10.1061/JGGEFK.GTENG-10636

Publication date
2023

Document Version
Final published version

Published in
Journal of Geotechnical and Geoenvironmental Engineering

ASCE

Pullout Capacity of Single and Biwing Anchors in a Soft Clay Deposit: Model Investigation in a Centrifuge and FEM Predictions

J. Fanning[1]; V. Sivakumar[2]; S. Nanda, Ph.D.[3]; K. Gavin[4]; T. Murray[5]; A. Bradshaw, M.ASCE[6]; J. Black[7]; and S. Jalilvand[8]

Abstract: One of the ways to install plate anchors in deep seabed is to drop the anchor system from the sea level and allow it to initially embed in the seabed under its own weight. Further dragging would cause the anchor to rotate and embed further into the seabed. There could be difficulties of getting the anchor plate horizontal or mooring line to be perpendicular to the plate where the maximum pullout capacity could be achieved. As part of the investigations, various aspects of the plate performance were examined through centrifuge testing in which the plate orientation and pullout angles were varied. It was presumed that dynamic stability of the anchor (during field installation) can be achieved by having the plate in biwing configuration. Therefore, the performance of the biwing anchors having different spacing between the plates was also examined in the centrifuge testing program and the findings were compared with predictions obtained through finite-element modeling (FEM). Both pullout directions and the plate angles considerably influenced the pullout capacity factors. The comparison between the predicted pullout capacity using FEM and measured pullout capacity for biwing anchors at shallow embedment depths was excellent. However, the FEM-predicted pullout capacity was noticeably lower than the measured ones for deep anchors. Pullout capacity of biwing anchors at shallow embedment depth increased as the spacing between the plates S increased from 0 to $0.5B$. However, there appears to be a slight reduction in the performance in deep embedment anchors. This is also reflected in FEM findings. **DOI: 10.1061/JGGEFK.GTENG-10636.**

Introduction

Monopiles have been used for 82% of all grid-connected offshore wind turbines (Wind Europe 2018). The major challenge with moving into deeper water is that conventional foundation solutions, such as monopiles, will become impractical and uneconomical due to the large environmental forces and the cost of installations. Efficient energy production relies on consistent and strong winds, which are often found further away from shorelines (Musial et al. 2004; Musial and Ram 2010). As the offshore wind industry begins to develop installations in areas of deeper water, the development of efficient and reliable foundation systems is necessary. To deploy wind turbines in these areas, the use of floating structures and mooring lines that are anchored to the seabed is the most economically feasible option (Musial et al. 2004).

To anchor mooring lines to the seabed, various options such as suction caissons or pile anchors are available and have been used in the offshore oil and gas industry (Randolph and Gourvenec 2011; Aubeny 2019). In these options, the pullout capacities generally result from side friction. However, the use of drag plate anchors could be an effective and attractive option due to their low installation costs and high holding capacity relative to their self-weight (Aubeny 2019). Vertically loaded anchors may be used for high vertical pullout requirements. The installation process of vertically loaded anchors is similar to the drag anchor. However, after the installation, using some mechanical arrangement, the angle between fluke and shank changes to around 90°; consequently, the anchor behaves as an embedded plate anchor with high pullout capacity (Aubeny 2019). The offshore oil and gas industry has used these anchors for both permanent and temporary moorings. Various experimental studies have been reported on drag anchors (Dunnavant and Kwan 1993; Neubecker and Randolph 1996a; Ozmutlu 2009; Liu et al. 2010b; Shin et al. 2011; Yu et al. 2015). Similarly, analytical studies have been reported (Lelievre and Tabatabaee 1981; Degenkamp and Dutta 1989; Stewart 1992; Neubecker and Randolph 1995, 1996b; Thorne 1998; O'Neill et al. 2003; Aubeny and Chi 2010; Liu et al. 2010a, 2012).

Plate anchors have been shown to provide an efficient and economical means of generating sufficient pullout capacity. The capacity of the anchor is dependent on the soil properties, embedment depth, anchor shape, orientation of anchor with the mooring line, and loading conditions (Merifield et al. 2001; Song et al. 2008;

[1]Senior Geotechnical Engineer, RPS, 74 Boucher Rd., Belfast BT12 6RZ, UK. Email: joseph.fanning@rpsgroup.com

[2]Reader in Geotechnical Engineering, School of Natural and Built Environment, Queen's Univ. Belfast, Belfast, BT7 1NN, UK (corresponding author). Email: v.sivakumar@qub.ac.uk

[3]Associate Professor, Kalinga Institute of Industrial Technology, India, Bhubaneswar 751024, India ORCID: https://orcid.org/0000-0002-6470-3771. Email: satyajeet.nandafce@kiit.ac.in

[4]Professor of Subsurface Engineering, Faculty of Engineering and Geosciences, TU-Delft, Stevinweg 1, PO box 5048, Delft, Netherlands. ORCID: https://orcid.org/0000-0002-0741-1115. Email: K.G.Gavin@tudelft.nl

[5]Consultant, Murray Rix Limited, Stoke Golding SK16 4QX, UK. Email: tedethiopia@murrayrix.co.uk

[6]Professor, Dept. of Civil and Environmental Engineering, Univ. of Rhode Island, Kingston, RI 02881. Email: abrads@uri.edu

[7]Lecturer in Geotechnical Engineering, Queen's Univ. Belfast, Belfast BT7 1NN, UK. Email: J.A.Black@qub.ac.uk

[8]Geotechnical Engineer, Gavin-Doherty Geosolutions Consulting Engineers, Dublin D14 X627, Ireland. Email: soroosh.jalilvand@ucdconnect.ie

Note. This manuscript was submitted on December 15, 2021; approved on March 2, 2023; published online on May 8, 2023. Discussion period open until October 8, 2023; separate discussions must be submitted for individual papers. This paper is part of the ***Journal of Geotechnical and Geoenvironmental Engineering***, © ASCE, ISSN 1090-0241.

Yang et al. 2010; Yu et al. 2015; Khatri and Kumar 2009). The techniques used to determine the pullout capacity of buried anchors are mostly based on empirical or semiempirical relationships. Anchor capacity in clays is typically presented as a dimensionless breakout factor, N_c [Eq. (1)]

$$N_c = \frac{Q_u}{A \cdot c_u} \tag{1}$$

where N_c = bearing capacity factor; Q_u = ultimate pullout load; A = anchor face area/fluke or plate area (the former is used in the rest of the article); and c_u = undrained shear strength of overlying soil. In this article, c_u is defined as the undrained strength at the embedment depth of the anchor. From upper- and lower-bound solutions, Merifield et al. (2001) suggested the breakout factor would be around 11.16–11.86. Song et al. (2008) reported the breakout factors for strip and circular anchors are 11.7 and 13.7, respectively. From the upper-bound (or lower-bound) solution, Martin and Randolph (2001) reported that the breakout factors are 10.28 and 13.11, respectively, for a strip plate anchor. The anchor roughness influences the breakout factor. The rough anchor possesses a high pullout capacity compared with the smooth anchor (Martin and Randolph 2001; Song et al. 2008; Merifield et al. 2001). Loading patterns also influence the breakout factor. Yu et al. (2015) observed that under cyclic loading, the pullout capacity is reduced by 20% compared with static loading. Khatri and Kumar (2009) reported that the breakout factor continuously increases with embedment until it reaches the critical embedment ratio. The breakout factor is not sensitive to the rate of increase in shear strength of soil strata. Considering six degrees of freedom (three force components and three moment components), Yang et al. (2010) noticed that the breakout factors for normal load, parallel load, in-plane moment, out-of-plane moment, and torsion are 12.5, 2, 1.9, 1.9, and 0.765, respectively.

The influence of anchor depth can be considered using a normalized embedment ratio such as $Er = H/B$, where H is the anchor embedment depth and B is the anchor width for the plates. Based on the embedment, the anchor can be classified as deep or shallow anchor. The deep anchor possesses a local failure mechanism, whereas the failure of the shallow anchor extends to the ground surface. From a finite-element modeling (FEM) study, Song et al. (2008) observed that a strip anchor became a deep anchor when H/B is more than 2. Merifield et al. (2001) reported soil shear strength influences the failure mechanism of the plate anchor and suggested that the anchors behave deep when $(\gamma H)/c_u$ is greater than 7. Chen et al. (2016) carried out centrifuge modeling to analyze the vertical pullout behavior of plate anchors at different depths in normally consolidated clay. The capacity factor stays essentially the same as the anchor depth increases beyond this critical depth. This was further explored by Yu et al. (2011), who carried out a two-dimensional finite-element analysis to determine the pullout capacity in uniform and normally consolidated clays, and the analysis was experimentally validated using data obtained from centrifuge testing carried out by Chen et al. (2016). The orientation of the anchor with the mooring line influences the anchor pullout capacity. The inclination of the anchor and mooring line angle to the surface influence the pullout capacity (Das and Puri 1989; Cassidy et al. 2012; Yang et al. 2012; Hu et al. 2021). Das and Puri (1989) observed that the pullout capacity increases with anchor inclination at embedment up to H/B of 3.

Fig. 1 outlines the installation procedure for a possible field application of drop and drag biwing plate anchors. The plate anchor could be dropped from a height above the seabed and would initially embed in the soil under the force of its own self-weight (Stage 1). Upon application of tension in the mooring line, keying of the anchor would then begin until the anchor had rotated to an orientation that would allow it to begin to further embed during dragging (Stage 2). Until this point, the fluke and shank are held closed by a coupling mechanism (Flores 2016). As the anchor fluke is rotated, this mechanism would release and allow the fluke and shank to open, enabling drag embedment of the anchor to occur. Dragging the anchor would cause the anchor fluke to rotate toward a horizontal orientation and embed further into the soil (Stage 3). This would enable the anchor to develop a higher holding capacity. References to each of the stages are given in Fig. 1. The concept of the proposed biwing plate anchors is a combination of dynamically

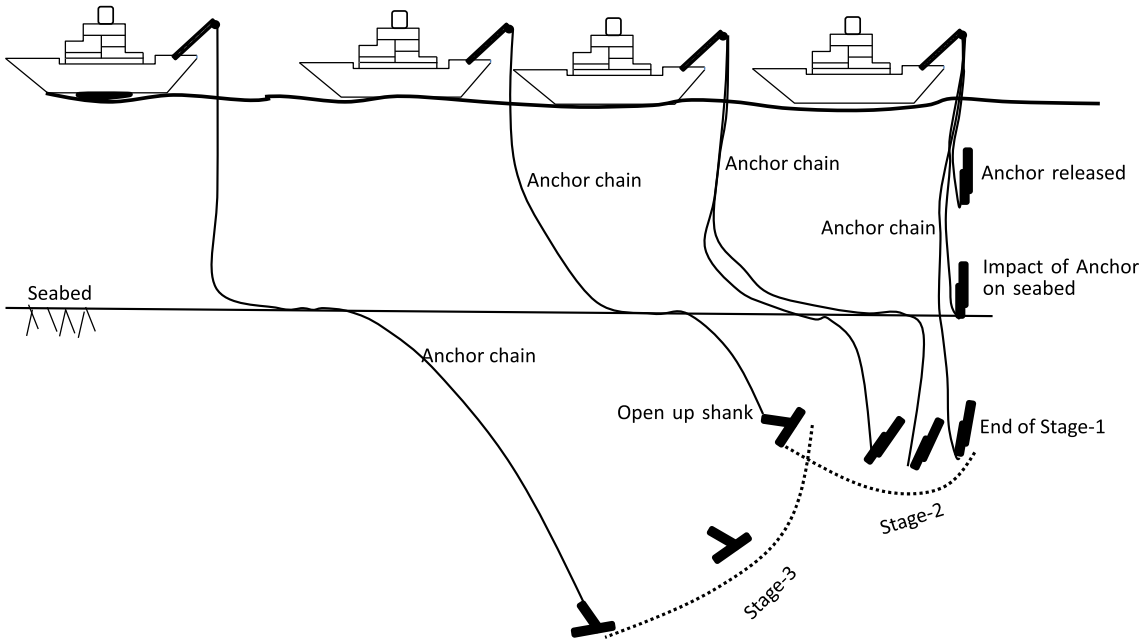

Fig. 1. Installation procedure for the plate anchor with separate stages highlighted. Stage 1 drop, Stage 2 keying, and Stage 3 drag embedment.

J. Geotech. Geoenviron. Eng., 2023, 149(7): 04023050

installed torpedo anchor (O'Loughlin et al. 2013; Richardson et al. 2009) and drag anchor (Aubeny and Chi 2010; O'Neill et al. 2003).

As a result of the complex drag anchor shapes and soil failure mechanisms during drag installation, the development of predictive models is highly dependent on the use of physical modeling. Due to the high cost of full-scale trials and large number of variables that influence the drag embedment of anchors, laboratory-based tests are an important part of the analysis of drag behavior. The research teams operating at Queen's University Belfast (QUB), University College Dublin, University of Texas, and University of Rhode Island were involved in performing a wide range of investigations to develop an anchor system for the offshore wind industry. One important aspect of this work is to explore ways of installing such devices in soft clay in deep seas effectively and efficiently. One of the approaches adopted was to examine the penetration of an anchor in the soil upon free fall from the surface (Fig. 1) and the subsequent dragging to get the anchor deeper into the soil deposit and rotate it to a near-horizontal orientation.

In a complementary investigation (not reported in this article, but the findings can be accessed through Fanning 2020) the installation procedure was modeled in a laboratory environment using water-based transparent material known as laponite. During the investigations, a high-speed camara was used to capture all three stages of the installation process illustrated in Fig. 1. Fig. 2 shows selected still images: Fig. 2(a) shows the initial penetration of the anchor (Stage 1), Fig. 2(b) the keying and shank opening (Stage 2), and Fig. 2(c) the final embedment upon further dragging (Stage 3). It is apparent that the final embedded anchor may not be horizontal or the mooring line perpendicular to the plate. Therefore, it is important to know the relevant pullout capacities under different orientations that can assist the designer to provide some safety margins on the stability of the wind platforms. The dynamic stability of the anchor during the free fall from the sea is also essential (Gerkus 2016). It can be achieved by having a multiple-plate system (in the present investigation, biwing anchors) that could also enhance the pullout capacity due to possible arching effects between the plates. The purpose of this article, therefore, is to explore these aspects through physical modeling carried out in centrifuge testing and validate the performance of the biwing plate anchor system using FEM analysis. The biwing plate anchor represents a split fluke anchor. The fluke has been split into two parts. It is considered that the resistance in the gap between the flukes devolved due to the bridging effect induced by the interaction of two split flukes. It can be anticipated that the biwing anchor shall achieve more penetration in Stage 1 because the total side frictional resistance is reduced due to the split in the fluke. The weight of the biwing anchor shall be less compared with the traditional anchor (although the projected area remains same). Therefore, more anchors can be transported to the construction site.

Physical Modeling

Pullout capacities of single square-plate and biwing anchors were investigated using physical modeling in a centrifuge. The investigations were carried out in a normally consolidated bed of kaolin clay. The anchor plates with widths $B = 20$ mm (scaling to 2 m) were idealized as wished in place (installed with the clay bed prepared around them) with embedment depths of 40 and 80 mm

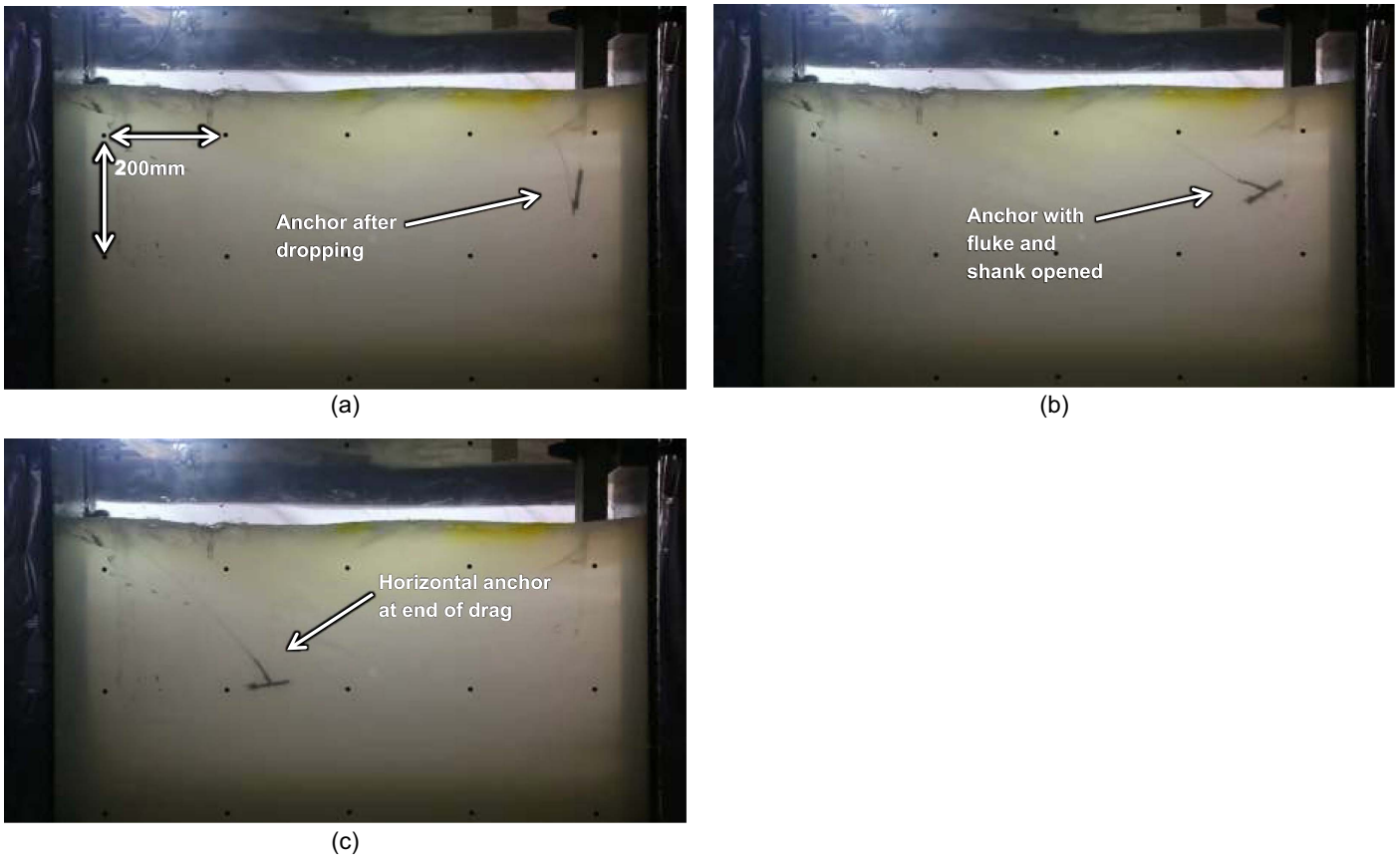

Fig. 2. Drop/drag anchor at different stages during test: (a) immediately after dropping; (b) fluke and shank opened after keying; and (c) anchor after completion of dragging (Test 1).

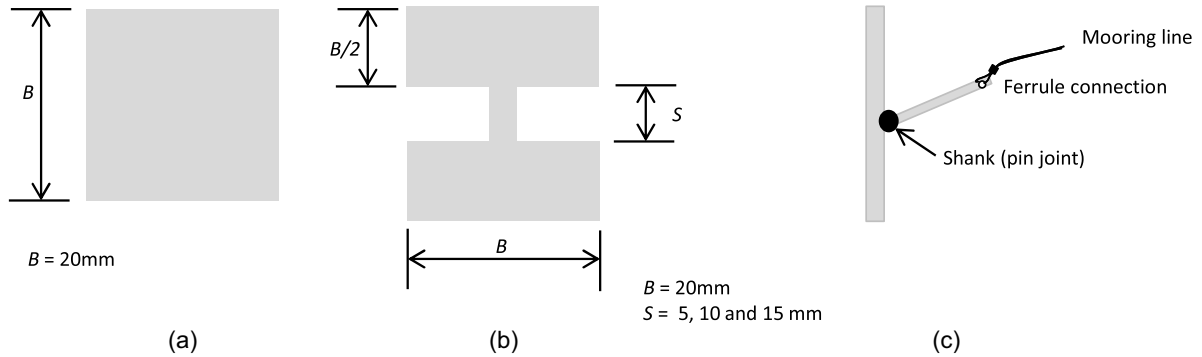

Fig. 3. Anchor shapes: (a) square plate; (b) biwing plate; and (c) side view.

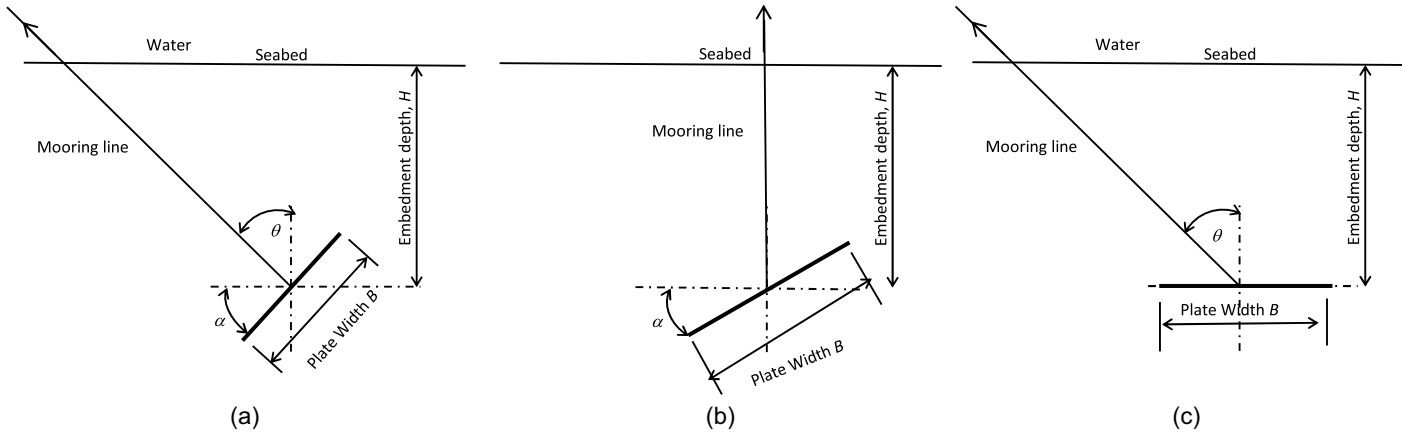

Fig. 4. Testing configurations (centrifuge testing): (a) plate angle (loading right angle to plate); (b) plate angle (loading vertical); and (c) loading angle (plate horizontal).

(scaling to 4 and 8 m). Approximate mass of the anchor was 5.0 g. The embedment ratios, E_r, for the full-scale plates $B = 2$ m would be 2 and 4, respectively, for 4- and 8-m embedment depth. The shapes of model anchors used in the tests are shown in Fig. 3. The plate was connected to a shank using a pin joint. The mooring line attachment to the shank was ferrule type. Because the size of this connection is less than 3 mm in diameter, any effects of this on the overall performance of the anchor is negligible. The first series of tests examined the effect of embedment ratio, anchor angle, and pullout angle on the pullout behavior of square plates $(S/B = 0)$. The tests carried out were (1) plate angle α being 0°, 20°, and 40° and the pullout angle being perpendicular to the plate [Fig. 4(a)]; (2) plate angle α being 0°, 20°, and 40° but the pullout angle θ being zero [vertical pullout, Fig. 4(b)]; and (3) plate angle α being zero and pullout angle θ being 0°, 20°, and 40° [Fig. 4(c)]. Both square and biwing plates were used in the test to examine the effect of varying S [spacing between the biwing plate anchor, as shown in Fig. 3(b)] on the vertical pullout capacity while the plate angle α was zero. The central spacings of the plates of the biwing anchors were $0.25B$, $0.5B$, and $0.75B$, representing model distances of 5, 10, and 15 mm. The shank and mooring line were attached to the plate as shown in Fig. 3(c).

Apparatus

The centrifuge modeling was carried out at the Centre for Energy and Infrastructure Ground Research at the University of Sheffield (Black 2014). The diameter of the rotating arm was 1.2 m. The models were prepared in an aluminum container that held the sample, with dimensions of 160 mm (length) by 100 mm (width) by 130 mm (height). The details of the test box and instrumentation are shown in Fig. 5. An actuator and pulley system were used to apply the pullout load. A movable pulley allowed the angle of pullout to be changed without having to place the plate close to the end boundaries. Due to the position of the load cell, a series of calibration tests were carried out to determine the friction between the pulley and the mooring line. The displacement of the embedded plate was measured using a displacement gauge attached to a plate behind the load cell shown in Fig. 5. A high-strength wire (mooring line) was used to attach the plate (via shank, Fig. 3) to the load cell, and it was shown that the extension of this wire under the range of measured loads was negligible.

Sample Preparation

Speswhite (Azelis UK, Newcastle, UK) kaolin clay was prepared at 1.5 times the liquid limit. Its liquid limit, plastic limit, and specific gravity were 71%, 31%, and 2.65, respectively (Table 1). Drainage was permitted from the top and bottom of the box. The base of the box was covered in a 5-mm layer of sand, and a layer of clay was then carefully placed in the chamber. A guide was then used to place the anchor plate at the correct orientation and position in the box with the mooring line attached. The location of the plate was at least $2B$ between the edges of the plates and the nearest

J. Geotech. Geoenviron. Eng., 2023, 149(7): 04023050

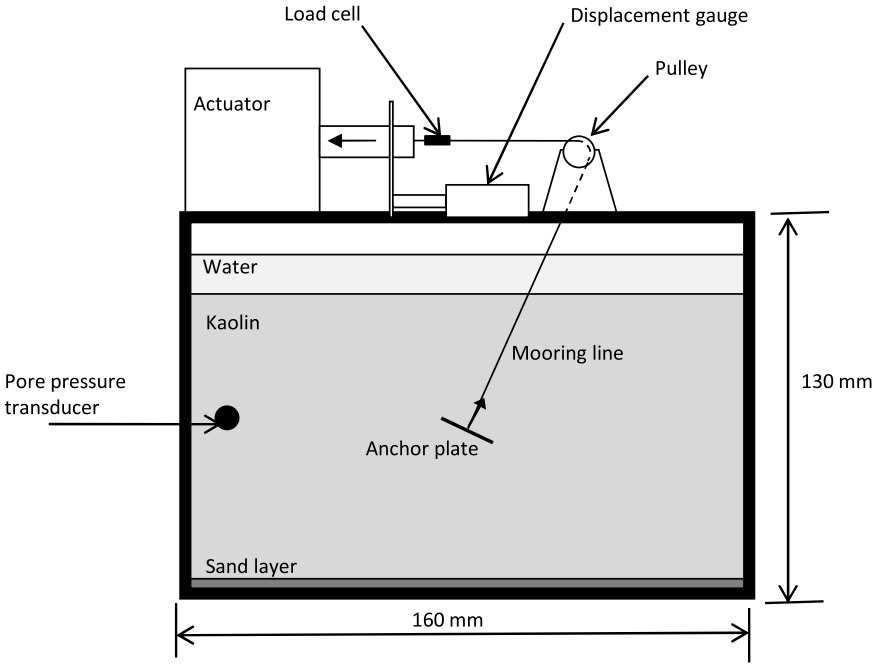

Fig. 5. Testing chamber in centrifuge.

Table 1. Model parameters for centrifuge testing and FEM

Physical property	Value
Liquid limit (%)	71
Plastic limit (%)	31
Specific gravity	2.65
Coefficient of consolidation (m^2/year)	6.5
E/c_u	500
Poisson's ratio, ν	0.49

boundary. The box was then filled with clay and a nominal head of water. The anchor mooring line was left free at the surface to allow the plate to move with the soil during consolidation. A miniature pressure transducer located at the midpoint of the sample height was used to measure the dissipation of the excess pore water pressure. The box was placed on the centrifuge and spun at $100g$ (where g is the gravitational acceleration) for 2 h. After this time, a thin needle was used to check the depth of the plate (at four locations) approximately from the clay surface and inclination of the plate was corrected if necessary for the intended test. The sample was then topped up to the target depth and the anchor mooring line was attached to the pullout mechanism with a small amount of slack to allow for further settlement. The sample was then reconsolidated at $100g$ until the pore pressure within the sample reached a plateau. During consolidation, a camera on the centrifuge was used to monitor the surface level of the clay and determine the final sample height.

Testing

Consolidation of the clay bed was completed within about 4 h from the beginning of the centrifugal action. At this stage, the pullout of the anchors was initiated. A pullout rate was determined using the equation $V = vd/c_v > 30$ from Finnie and Randolph (1994). In this equation, V represents the dimensionless velocity, v is the pullout velocity, d is the equivalent diameter of the plate, and c_v is the coefficient of consolidation of the clay. Using this equation, a pullout strain rate of 3 mm/s was chosen to ensure undrained conditions during the pullout process. As a result of using air pressure to move the actuator, the rate of anchor displacement could only be controlled until the anchor achieved its peak capacity. After this point, the displacement rate of the plate was uncontrolled. The point at which the slack in the wire was taken in and the displacement of the plate started was apparent through a noticeable change in the load cell output.

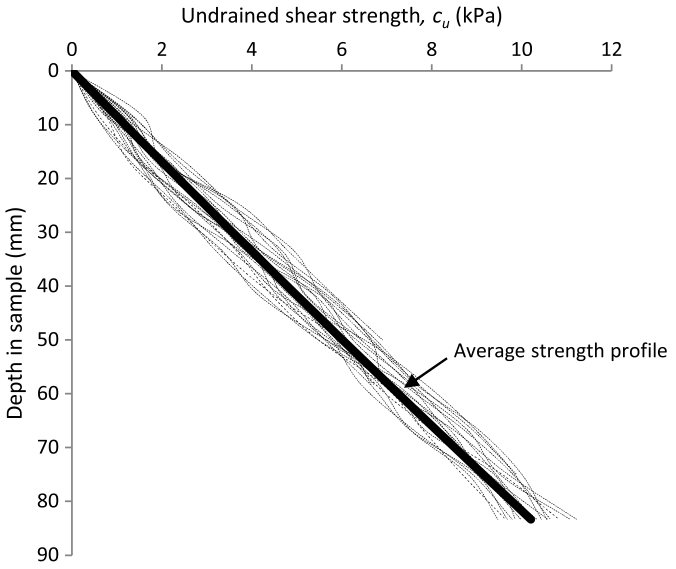

Fig. 6. Undrained shear strength profile.

Undrained Shear Strength (c_u) Profile

Upon completion of the pullout, the undrained shear strength profile of the sample was determined using a precalibrated cone penetrometer. Fig. 6 shows the shear strength profiles for each test

sample. The shear strength, c_u, increased linearly with depth at a rate of 0.17 kPa/kPa at full scale (this agrees with the predicted undrained shear strength using Skempton's formulation with liquid limit of 71% and plastic limit of 31%). Samples were also taken after each test to determine the moisture content profile and bulk density. This was carried out to help ensure repeatability of the tests [further information on these parameters can be found in Fanning (2020)].

FEM Analysis

A three-dimensional finite-element analysis was conducted to study the pullout behavior of biwing and plate anchors and compare it with the centrifuge experiments. The coupled Eulerian Lagrangian (CEL) technique in ABAQUS/Explicit was employed. This enabled the assessment of the effect of large-deformation phenomena (such as cavity formation and closure behind the anchor) on the pullout response. The soil behavior was simulated using the Tresca criterion as an elastic-perfectly plastic material with uniform undrained shear strength corresponding to its value at the initial embedment depth of the anchor in the centrifuge tests. The Young's modulus E was assumed to be directly proportional to the undrained shear strength with a ratio of $E/c_u = 500$ adopted. A Poisson's ratio (ν) of 0.49 was used to model the constant-volume behavior under undrained conditions. The anchor was modeled as a rigid plate.

Two plate anchor configurations were considered: (1) a square-plate anchor of width $B = 2$ m, $S = 0$; and (2) two rectangular-plate anchors with dimensions 2×1 m (i.e., $B \times 0.5B$) separated at a distance of $S = 0.0B, 0.25B$, and $0.50B$. Due to time limitations because the investigations were carried out away from the hosting institution (QUB), $S = 0.75B$ was not included in the FEM. The soil domain size was selected to be large enough to eliminate any boundary effects. The boundary conditions were fixed such that material movement was constrained in directions normal to the domain faces. Due to the symmetry of plate anchors, only half of the model was considered in the analysis. A typical finite-element mesh used in the pullout analysis is shown in Fig. 7 where a minimum mesh size of $B/40$ was adopted in the region surrounding the plate anchor. The simulation procedure involved the following steps:

1. The plate anchor was embedded (wished in place) at the depth H below the soil (embedment ratio of 2 and 4).
2. An initial equilibrium analysis was conducted to establish geostatic stresses in the soil bed.
3. A pullout analysis was conducted by moving the anchor in the vertical direction at a constant rate of $0.02B/\text{s}$. The pullout rate was selected such that the inertial effects introduced in the model due to the use of and artificial time scale (associated with an ABAQUA/Explicit approach) were eliminated.

The outputs extracted from the pullout analysis included the resistance force applied to the anchor, F, the corresponding anchor displacement, w, and the incremental displacement of soil material. The pullout capacity factor, N_c, was determined as the ratio of the peak pullout force ($F_{\max}$) to the area of the plate anchor (A) and the undrained shear strength (c_u) according to $N_c = F_{\max}/Ac_u$. The anchor failure mechanism was assessed through the study of the soil movement in the vicinity of the anchor.

Results and Discussion

Physical Modeling in Centrifuge

Effect of Embedment Ratio

Fig. 8 shows the normalized pullout behavior of horizontal square-plate anchors at embedment ratios of 2 and 4. These plates were located horizontally and pullout force was applied vertically (i.e., $\theta = \alpha = 0°$). At an embedment ratio of 2, a bearing capacity factor of 11.2 was measured. The two tests carried out with the anchor at an embedment ratio of 4 provided bearing capacity factors of 12.4 and 12.5, indicating the repeatability of the results. The capacities at an embedment ratio of 4 matched the findings of the centrifuge modeling carried out by Chen et al. (2016), which found the limiting capacity for square anchors to be 12.5.

Effect of Pullout Angle with Inclined Plates

Fig. 9 shows the pullout behavior of the square-plate anchor with the angle of pull θ at 0°, 20°, and 40° to the vertical. The anchor plate angle was zero [i.e., oriented normal to the direction of pull for each of the tests so that $\alpha = \theta$ in Fig. 4(a)]. The greatest breakout factor was obtained for a vertical pullout ($\alpha = \theta = 0$), with the

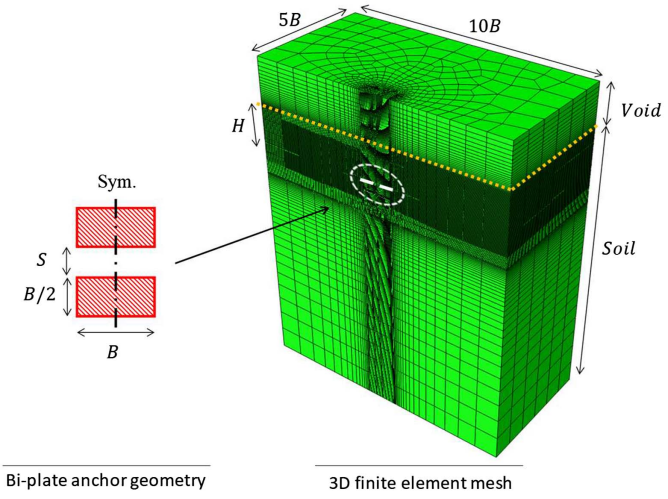

Fig. 7. Typical finite-element mesh used in the numerical analysis of the pullout.

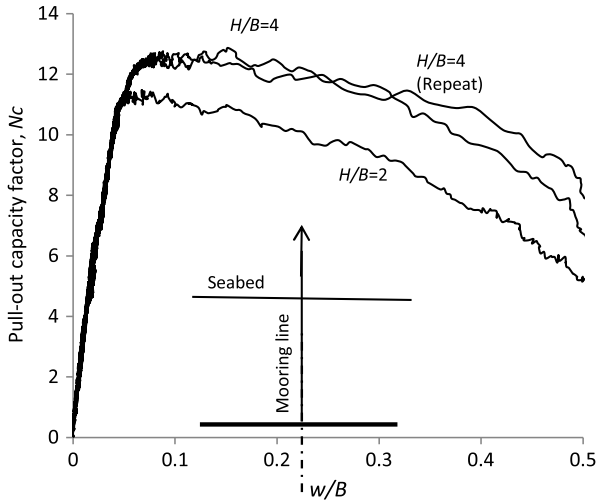

Fig. 8. Pullout capacity versus vertical displacement for a square plate at embedment ratios of 2 and 4 (horizontal plate, vertical pullout), centrifuge testing.

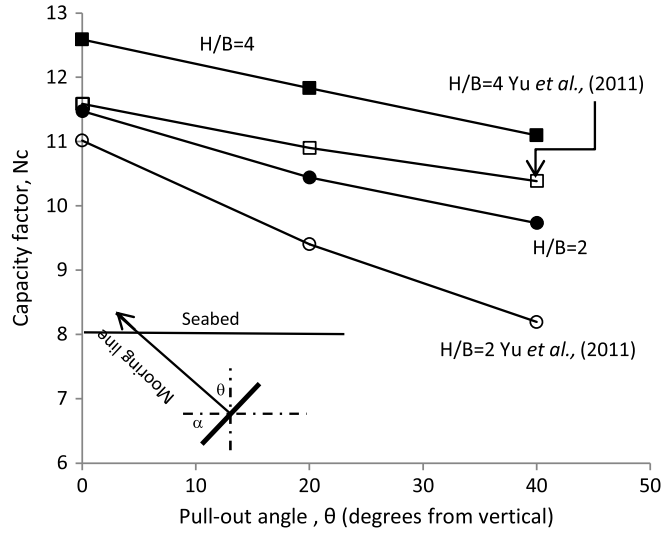

Fig. 9. Pullout capacity versus loading orientation with anchor plates normal to the angle of pull (centrifuge testing).

capacity decreasing as the pullout angle moved toward the horizontal at embedment ratios of 2 and 4. This trend agrees with the findings of previous studies such as Chen et al. (2016). The same trend is shown by the numerical model of Yu et al. (2011) but the breakout factors obtained in the current study were consistently higher than those predicted by Yu et al. (2011). This is considered as possibly due to the numerical model being generated for two-dimensional strip anchors.

Effect of Plate Angle with Vertical Loading

The effect of varying the angle of the square plate with respect to the horizontal α is shown in Fig. 10. As discussed previously, when the plate is normal to the direction of pull, the peak capacity is achieved. As the plate rotated and the pullout direction was kept vertical, the capacity decreased due to a reduced projected area of the anchor in the direction of pull and the pullout capacity relied on the adhesion developed at the interface between the anchor and the surrounding soil. In the tests carried out at an embedment ratio of 2, the anchor capacities at angles to the horizontal of 20° and 40° were 91% and 66% of the horizontal capacity, respectively. At an embedment ratio of 4, the capacities at 20° and 40° were 80% and 67% of the horizontal capacity, respectively. This study was conducted only at plate angles of 20° and 40° and therefore more study is required to quantify the rate of change of anchor capacity with plate angle.

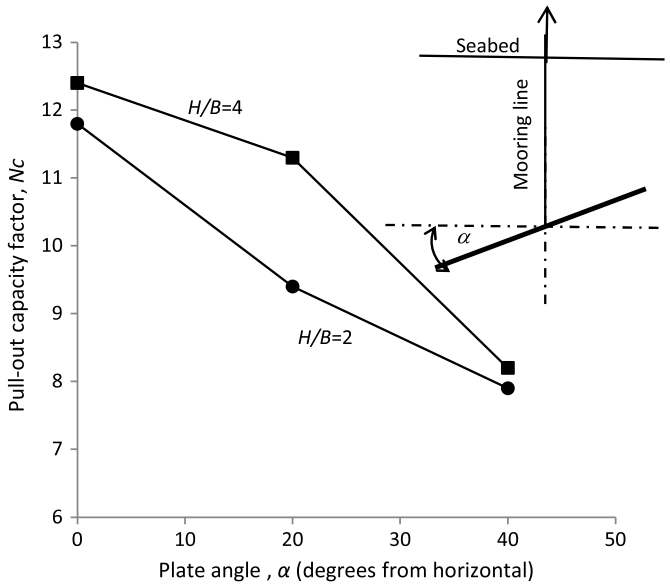

Fig. 10. Pullout capacity versus varying plate angle under vertical pullout (centrifuge testing).

Effect of Pullout Angle with Horizontal Plates

Fig. 11 shows the effect of increasing the pullout angle θ from 0° to the vertical to 20° and 40° for a horizontal square-plate anchor at an embedment ratio of 2. As expected, the capacity factor decreases as the angle of pull is increased. This is due to the increasing reliance of the anchor on the adhesion between the plate and surrounding soil. At an angle of 40°, the anchor began to drag through the soil, and this resulted in a large decrease in N_c. This significant decrease in N_c was not observed when the anchor pullout was kept vertical, and also when the plate was inclined at 40° to the horizontal (Fig. 10). Further tests are needed to confirm these findings.

Effect of Plate Spacing

The load–displacement behavior of the anchors at embedment ratios of 2 and 4 are shown in Figs. 12(a and b), respectively. The load–displacement behaviors at both embedment depths are reasonably comparable before a peak capacity was achieved. However, the postpeak behavior of the shallow anchors shows a greater degree of strain softening as opposed to the anchors embedded at a greater depth (this is indicated by the slopes of postpeak stress–strain curves). At a shallow embedment depth, the increase in capacity with increasing S/B can be explained in terms of interference between the biwing anchor plates. This was found to be the case in fine soils as reported by Sahoo and Kumar (2014) among others. Their work showed that as the space between two anchor plates increased, the anchor capacity increased until a critical spacing was reached when the anchor capacity plateaued. They also showed that at greater embedment depths, the increased overburden pressure meant that a greater space between the anchor plates was required to result in an increase in the capacity.

Fig. 13 shows the effect of increasing the spacing S between the two halves of the split-square anchor plate. As the spacing between the plates increased, the pullout factor of the anchor at an embedment ratio of 2 increased from 11.5 to a maximum of 12.0. As the spacing increased beyond $S = 0.5B$, the capacity factor did not increase and exhibited a small decrease in capacity. The pullout factor for the anchors at an embedment ratio of 4 did not change noticeably as the spacing S increased from 0 to $0.5B$ with values of N_c remaining between 12.4 and 12.6, though perhaps again showing a small decrease in capacity beyond $S = 0.5B$.

Numerical Modeling

The results of the numerical analysis are first presented here and the comparison with the laboratory investigations are discussed subsequently. The value of the normalized overburden pressure–strength ratio, $\gamma' H/c_u$ (where γ' is effective unit weight of clay), in the laboratory tests was approximately 5.3 based on the relationship between the undrained shear strength at the embedment depth, the embedment depth of the anchor in the centrifuge, and the effective unit weight of the clay. The value of $\gamma' H/c_u$ in the numerical analysis was varied between 4.0 and 8.0 to investigate an upper and a lower range of undrained shear strength parameters.

Fig. 14 shows the results of pullout analysis for biwing anchors with the interplate spacing of $S/B = 0$, 0.25, and 0.50 and the

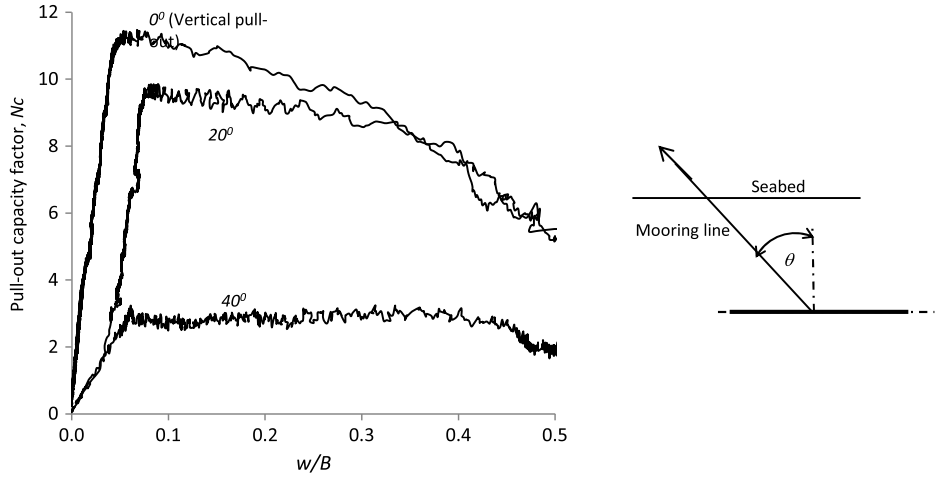

Fig. 11. Pullout capacity versus displacement for horizontal square-plate anchors with a varying angle of pull (centrifuge testing).

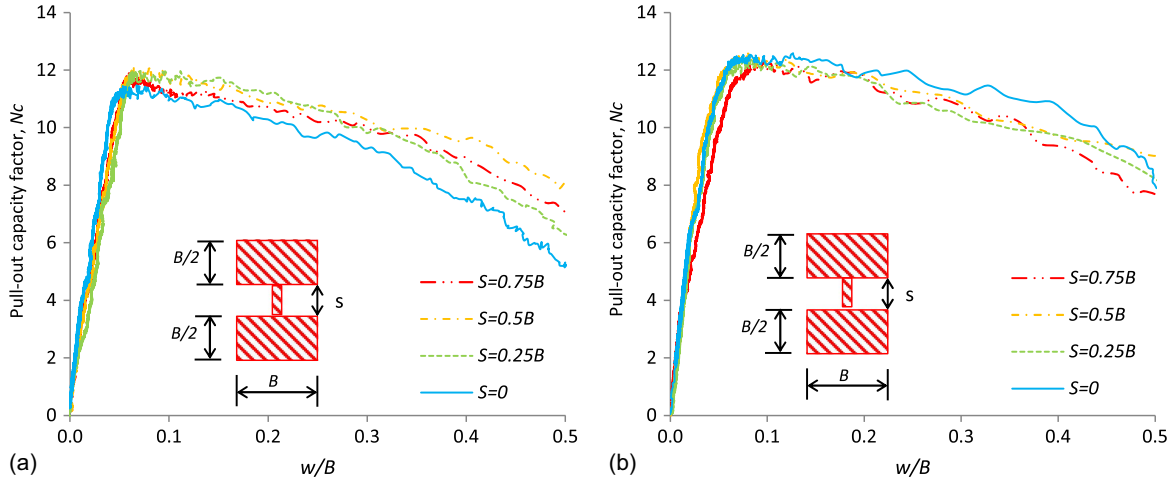

Fig. 12. Pullout capacity versus displacement for different plate spacing at embedment ratios of (a) 2; and (b) 4.

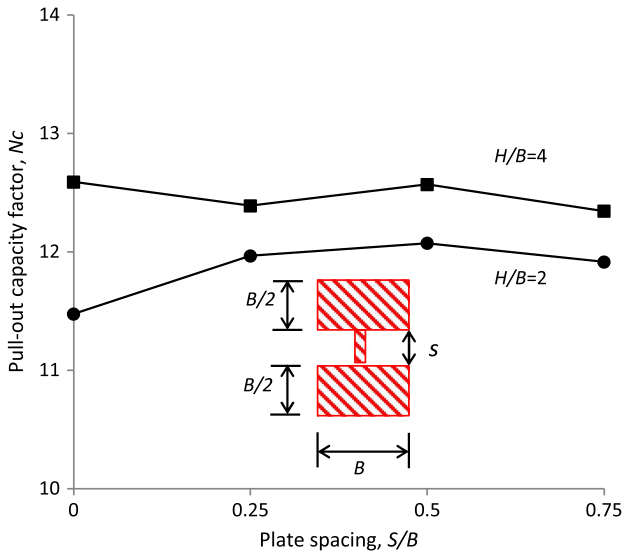

Fig. 13. Pullout capacity versus plate spacing at embedment ratios of 2 and 4.

normalized overburden pressure–strength ratio of $\gamma' H/c_u = 4.0$ and 8.0. The data for zero interplate spacing correspond to the square single-plate anchor configuration. The results are presented in terms of the pullout force applied to the anchor normalized by the area of the plate anchor and the undrained shear strength (c_u) against the anchor displacement (w) normalized by the width of the anchor (w/B). The following trends are noteworthy:

- The soft clay with $\gamma' H/c_u = 8.0$ develops a slightly higher normalized pullout capacity than the stiffer clay with $\gamma' H/c_u = 4.0$.
- Larger displacements are required to mobilize the pullout capacity for $\gamma' H/c_u = 4.0$ as compared with $\gamma' H/c_u = 8.0$ at both shallow ($H/B = 2$) and deep ($H/B = 4$) embedment depths.
- The plate spacing had no effect on the failure mechanism developed as discussed subsequently.

The differences in capacity and displacement required to mobilize the resistance can be explained by the failure mode developed by the anchor during pullout tests. Generally, a deep failure mechanism is evident by rapid mobilization of resistance followed by a horizontal asymptote (with no softening). The soil flows around the anchor until the full-closure condition is achieved. For shallow embedment depth, postpeak softening can be expected in stiffer clays because cavity closure behind the anchor is unlikely to occur. From

J. Geotech. Geoenviron. Eng., 2023, 149(7): 04023050

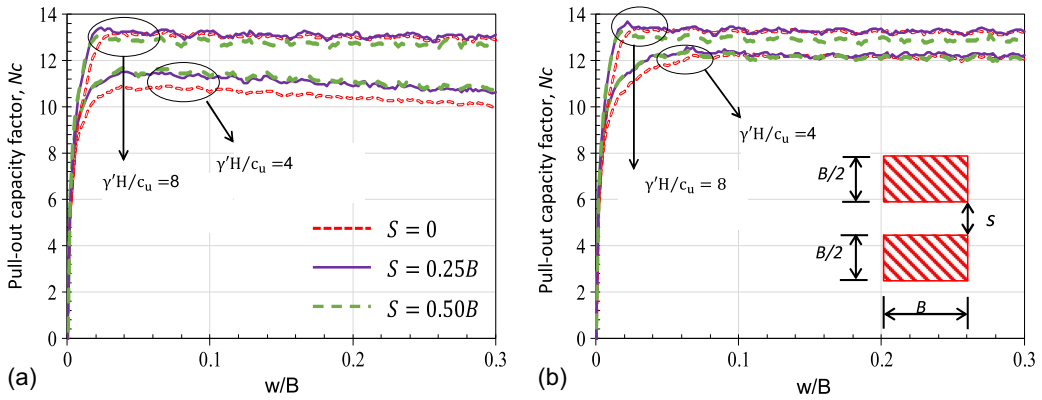

Fig. 14. Variation of pullout capacity versus displacement obtained from numerical analysis for biwing plate anchors with embedment ratios (a) $H/B = 2$; and (b) $H/B = 4$ (finite-element modeling).

the analyses undertaken, flow around the zone corresponding to the deep failure mechanism was achieved for the softer clay ($\gamma' H/c_u = 8.0$) even when the anchor embedment was $H/B = 2$ (i.e., shallow embedment). For the anchor in stiffer clay ($\gamma' H/c_u = 4.0$) at the shallow embedment depth [Fig. 14(a)], a shallow failure mechanism developed that extended to the soil surface and some postpeak loss of capacity was noticed. An intermediate anchor failure mode was identified for the stiffer clay at the higher embedment ratio, where only a small postpeak drop in resistance was observed and the flow mechanism allowed for a partial closure of the cavity behind the anchor.

Although Fig. 14 showed that for a biwing anchor the spacing did not affect the overall failure mechanism, the spacing did have some effect on the pullout capacity under certain conditions. This is investigated in Fig. 15 where the pullout capacity mobilized by the anchor under various combinations of (1) shallow and deep embedment ratios, (2) soft and stiff undrained shear strength, and (3) single- or biwing anchor configurations are presented. The value of the pullout capacity in Fig. 14 is calculated according to

$$\frac{F_{\max} + \gamma' \mathrm{Vol}}{A c_u} = N_c + \frac{\gamma' V}{A c_u} \tag{2}$$

where Vol = volume of the anchor; N_c = anchor capacity factor directly obtained from the pullout simulation; and $\gamma' \mathrm{Vol}/A c_u$ = correction factor. The application of the correction factor allows for the elimination of the buoyancy effect (i.e., geostatic pressure gradient between the top and bottom faces of the anchor) in the determination of the anchor capacity.

It can be seen that the normalized resistance is highest for the deep anchor mechanism and lowest for the shallow anchor response. The variation of the pullout capacity decreases as the interplate spacing increases. This is because the pullout capacity remains relatively constant for changes in the interplate spacing for the intermediate and deep modes of failure, while it increases with the interplate spacing for the shallow mechanism. This is explained by the fact that the intermediate and deep anchor behaviors are governed by partially and fully localized failure mechanisms that show little dependence on the anchor geometry, while the shallow anchor behavior is governed by a failure mechanism that extends from the anchor toward the soil surface and therefore is more greatly linked to the anchor geometry. As the interplate spacing increases, the anchor geometry diverges from a square-plate anchor and gradually converges to two rectangular-plate anchors. The slight decrease in the pullout capacity for the deep anchor mechanism is therefore expected because the flow-around mechanism mobilized under this mode of failure results in a slightly smaller

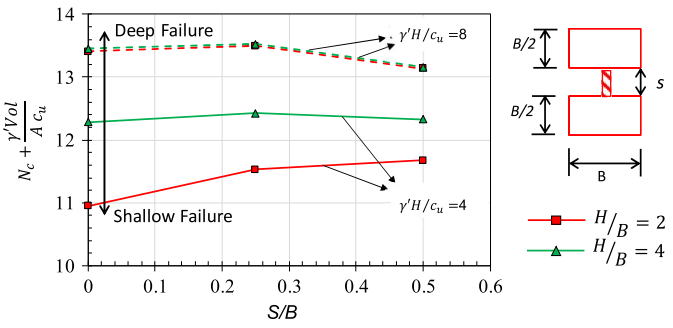

Fig. 15. Variation of the pullout capacity with the interplate spacing determined from numerical analysis for stiff ($\gamma' H/c_u = 4$) and soft ($\gamma' H/c_u = 8$) soil conditions (finite-element modeling).

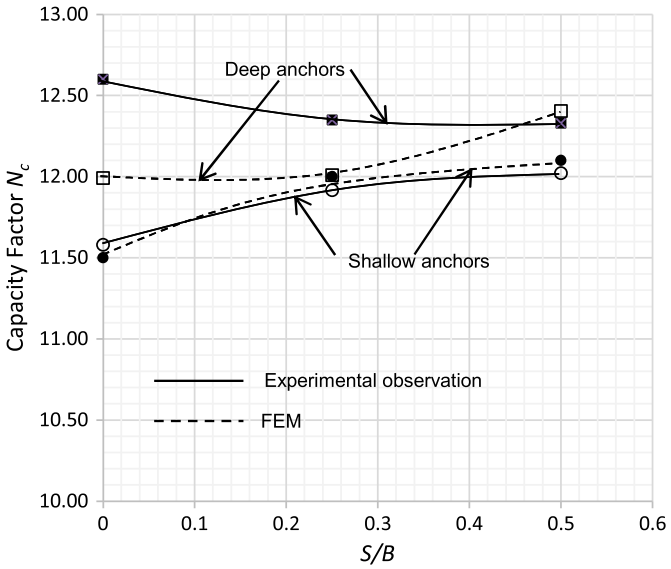

Fig. 16. Comparison of normalized pullout capacity factor (biwing anchor) between FEM modeling and experimental observations.

pullout capacity for the rectangular-plate anchors as compared with the square-plate anchors. The increase in the pullout capacity for the shallow mechanism is also expected and is explained in terms of the failure mechanism that is governed by both the weight of the soil block overlying the anchor as well as the shear stress developed along the perimeter of the anchor and extending to the soil surface. As the interplate spacing increases, the anchor perimeter length gradually increases, which is associated with a larger failure surface.

Comparisons of pullout capacities predicted using FEM and measured in the centrifuge testing for biwing anchors are presented in Fig. 16. FEM analysis considered $\gamma' H/c_u$ ratios of 4.0 and 8.0, representing stiff and soft clay deposits, respectively. The pullout capacities obtained for these ratios are interpolated for $\gamma' H/c_u = 5.3$, an approximate value attained for centrifuge model testing. Both FEM predictions and experimental observations agree exceptionally well for the pullout capacities of shallow-embedment biwing anchors where the capacities increased with the spacing between the plates and reached a plateau at S/B ratio of 0.5. However, the differences between the FEM predictions and experimental observations are significant in the case of deep anchors with lower pullout capacities predicted using FEM.

Conclusion

In this article, the pullout behavior of anchor plates (both single and biwing) in normally consolidated clay was analyzed through centrifuge testing and FEM modeling (only in the case of biwing). The centrifuge modeling was used to validate FEM analysis of the effect of varying the spacing between two anchor flukes on the pullout capacity of a novel biwing anchor. The following conclusions can be drawn from this study:

1. Interplate spacing had minimal effect on deep soil failure mechanisms. However, for shallow-soil failure mechanisms, increasing the interplate spacing resulted in an increased capacity on the order of 6%.
2. The centrifuge modeling was also used to analyze the effect of anchor orientation and pullout direction on the anchor capacity.
   - As expected, for all arrangements examined (horizontal plate under normal pullout, inclined plates under normal pullout, and inclined plates under vertical pullout), normalized capacity was greater for a deep failure mechanism than a shallow mechanism.
   - Normalized capacity decreased as the anchor inclination moved from a horizontal orientation toward a vertical one for both shallow and deep failure mechanisms. If the direction of pull is vertical instead of normal to the plate, the reduction is greater due to the reduced projected area of the anchor in the direction of loading.
3. FEM analysis suggested that biwing anchor provides a marginally better performance in shallow anchors, which agrees with the experimental observations. There appears to be no significant benefit in biwing anchors in deep embedment (FEM analysis).
4. The agreement between the predicted (FEM) and measured pullout capacities is found to be excellent in the case of shallow biwing anchors having a range of spacings between the two plates.

Data Availability Statement

Some or all data, models, or code that support the findings of this study are available from the corresponding author upon reasonable request.

Acknowledgments

The funding for the project was provided by the Department for Learning and Employment, Northern Ireland, UK under the US-Ireland R&D partnership (Grant No. USI-041).

References

Aubeny, C. 2019. *Geomechanics of marine anchors*. 1st ed. Boca Raton, FL: CRC Press.

Aubeny, C. P., and C. Chi. 2010. "Mechanics of drag embedment anchors in a soft seabed." *J. Geotech. Geoenviron. Eng.* 136 (1): 57–68. https://doi.org/10.1061/(ASCE)GT.1943-5606.0000198.

Black, J. 2014. "Establishing a 50H-ton geotechnical centrifuge at the University of Sheffield." In *Proc., 8th Int. Conf. on Physical Modelling in Geotechnics*. Boca Raton, FL: CRC Press.

Cassidy, M. J., C. Gaudin, M. F. Randolph, P. C. Wong, D. Wang, and Y. Tian. 2012. "A plasticity model to assess the keying of plate anchors." *Géotechnique* 62 (9): 825–836. https://doi.org/10.1680/geot.12.OG.009.

Chen, J., C. F. Leung, and Y. K. Chow. 2016. "Centrifuge model study on inclined pull-out behavior of square plate anchors in normally consolidated clay." In *Proc., Offshore Technology Conf.* Houston: Offshore Technology Conference.

Das, B. M., and V. K. Puri. 1989. "Holding capacity of inclined square plate anchors in clay." *Soils Found.* 29 (3): 138–144. https://doi.org/10.3208/sandf1972.29.3_138.

Degenkamp, G., and A. Dutta. 1989. "Soil resistances to embedded anchor chain in soft clay." *J. Geotech. Eng.* 115 (10): 1420–1438. https://doi.org/10.1061/(ASCE)0733-9410(1989)115:10(1420).

Dunnavant, T. W., and C. T. Kwan. 1993. "Centrifuge modelling and parametric analyses of drag anchor behavior." In *Proc., Offshore Technology Conf.* Houston: Offshore Technology Conference.

Fanning, J. 2020. "Plate anchors for offshore foundations in sand and clay." Ph.D. thesis, Queen's Univ. https://pure.qub.ac.uk/en/studentTheses/plate-anchors-for-offshore-foundations-in-sand-and-clay.

Finnie, I. M. S., and M. F. Randolph. 1994. "Punch-through and liquefaction induced failure of shallow foundations on calcareous sediments." In *Proc., Int. Conf. on Behaviour of Offshore Structures*, 217–230. Cambridge, UK: Geotechnics.

Flores, J. E. I. 2016. "Risk-informed design of new anchor concept for floating energy production systems." Ph.D. thesis, Dept. of Civil, Architectural, and Environmental Engineering, Univ. of Texas at Austin.

Gerkus, H. 2016. "Model experiments to measure yield thresholds and trajectories for plate anchors and develop a new anchor concept." Ph.D. thesis, Dept. of Civil, Architectural, and Environmental Engineering, Univ. of Texas at Austin.

Hu, C., J. Chen, C. F. Leung, Y. K. Chow, and Z. Li. 2021. "Pull-out mechanism of horizontal and inclined plate anchors in normally consolidated clay." *J. Mar. Sci. Eng.* 9 (10): 1103. https://doi.org/10.3390/jmse9101103.

Khatri, V. N., and J. Kumar. 2009. "Vertical uplift resistance of circular plate anchors in clays under undrained condition." *Comput. Geotech.* 36 (8): 1352–1359. https://doi.org/10.1016/j.compgeo.2009.06.008.

Lelievre, B., and J. Tabatabaee. 1981. "The performance of marine anchors with planar flukes in sand." *Can. Geotech. J.* 18 (Sep): 520–534. https://doi.org/10.1139/t81-063.

Liu, H., Y. Li, H. Yang, W. Zhang, and C. Liu. 2010a. "Analytical study on the ultimate embedment depth of drag anchors." *Ocean Eng.* 37 (6): 1292–1306. https://doi.org/10.1016/j.oceaneng.2010.06.007.

Liu, H., C. Liu, H. Yang, Y. Li, W. Zhang, and Z. Xiao. 2012. "A novel kinematic model for drag anchors in seabed soils." *Ocean Eng.* 49 (Aug): 33–42. https://doi.org/10.1016/j.oceaneng.2012.04.013.

Liu, H., W. Zhang, X. Zhang, and C. Liu. 2010b. "Experimental investigation on the penetration mechanism and kinematic behavior of drag anchors." *Appl. Ocean Res.* 32 (4): 434–442. https://doi.org/10.1016/j.apor.2010.09.004.

Martin, C. M., and M. F. Randolph. 2001. "Applications of the lower and upper bound theorems of plasticity to collapse of circular foundations." In *Proc., 10th Int. Conf. Int. Association for Computer Methods and Advances in Geomechanics*, 1417–1428. Boca Raton, FL: CRC Press.

Merifield, R. S., S. W. Sloan, and H. S. Yu. 2001. "Stability of plate anchors in undrained clay." *Géotechnique* 51 (2): 141–153. https://doi.org/10.1680/geot.2001.51.2.141.

Musial, W., S. Butterfield, and A. Boone. 2004. "Feasibility of floating platform systems for wind turbines." In *Proc., 42nd AIAA Aerospace Sciences Meeting and Exhibit*. Golden, CO: National Renewable Energy Lab.

Musial, W., and B. Ram. 2010. *Large-scale offshore wind power in the United States assessment of opportunities and barriers*. Golden, CO: National Renewable Energy Laboratory.

Neubecker, S. R., and M. F. Randolph. 1995. "Profile and frictional capacity of embedded anchor chains." *J. Geotech. Eng.* 121 (11). https://doi.org/10.1061/(ASCE)0733-9410(1995)121:11(797).

Neubecker, S. R., and M. F. Randolph. 1996a. "The kinematic behaviour of drag anchors in sand." *Can. Geotech. J.* 33 (4): 584–594. https://doi.org/10.1139/t96-084-306.

Neubecker, S. R., and M. F. Randolph. 1996b. "The static equilibrium of drag anchors in sand." *Can. Geotech. J.* 33 (4): 574–583. https://doi.org/10.1139/t96-083-305.

O'Loughlin, C. D., M. D. Richardson, M. F. Randolph, and C. Gaudin. 2013. "Penetration of dynamically installed anchors in clay." *Géotechnique* 63 (11): 909–919. https://doi.org/10.1680/geot.11.P.137.

O'Neill, M. P., M. F. Bransby, and M. F. Randolph. 2003. "Drag anchor fluke–soil interaction in clays." *Can. Geotech. J.* 40 (1): 78–94. https://doi.org/10.1139/t02-096.

Ozmutlu, S. 2009. "The value of model testing in understanding the behavior of offshore anchors: Towards new generation anchors." In *Proc., Offshore Technology Conf.* Houston: Offshore Technology Conference.

Randolph, M., and S. Gournevec. 2011. "Offshore geotechnical." In *Engineering*. 1st ed. Abingdon, UK: CRC Press.

Richardson, M. D., C. D. O'Loughlin, M. F. Randolph, and C. Gaudin. 2009. "Setup following installation of dynamic anchors in normally consolidated clay." *J. Geotech. Geoenviron. Eng.* 135 (4): 487–496. https://doi.org/10.1061/(ASCE)1090-0241(2009)135:4(487).

Sahoo, J. P., and J. Kumar. 2014. "Vertical uplift resistance of two interfering horizontal anchors in clay." *J. Geotech. Geoenviron. Eng.* 140 (4): 06013007. https://doi.org/10.1061/(ASCE)GT.1943-5606.0001073.

Shin, H. K., B. C. Seo, and J. H. Lee. 2011. "Experimental study of embedding motion and holding power of drag embedment type anchor on hard and soft seafloor." *Int. J. Nav. Archit. Ocean Eng.* 3 (3): 193–200. https://doi.org/10.2478/IJNAOE-2013-0062.

Song, Z., Y. Hu, and M. F. Randolph. 2008. "Numerical simulation of vertical pullout of plate anchors in clay." *J. Geotech. Geoenviron. Eng.* 134 (6): 866–875. https://doi.org/10.1061/(ASCE)1090-0241(2008)134:6(866).

Stewart, W. P. 1992. "Drag embedment anchor performance prediction in soft soils." In *Proc., 24th Mnuai OW*, 4–7. Houston: Offshore Technology Conference.

Thorne, C. P. 1998. "Penetration and load capacity of marine drag anchors in soft clay." *J. Geotech. Geoenviron. Eng.* 124 (10): 945–953. https://doi.org/10.1061/(ASCE)1090-0241(1998)124:10(945).

Wind Europe. 2018. *Offshore wind in Europe, key trends and statistics 2017*. Brussels, Belgium: Wind Europe.

Yang, M., C. P. Aubeny, and J. D. Murff. 2012. "Behaviour of suction embedded plate anchors during keying process." *J. Geotech. Geoenviron. Eng.* 138 (2): 174–183. https://doi.org/10.1061/(ASCE)GT.1943-5606.0000582.

Yang, M., J. D. Murff, and C. P. Aubeny. 2010. "Undrained capacity of plate anchors under general loading." *J. Geotech. Geoenviron. Eng.* 136 (10): 1383–1393. https://doi.org/10.1061/(ASCE)GT.1943-5606.0000343.

Yu, L., J. Liu, X. J. Kong, and Y. Hu. 2011. "Numerical study on plate anchor stability in clay." *Géotechnique* 61 (3): 235–246. https://doi.org/10.1680/geot.8.P.071.

Yu, L., Q. Zhou, and J. Liu. 2015. "Experimental study on the stability of plate anchors in clay under cyclic loading." *Theor. App. Mech. Lett.* 5 (2): 93–96. https://doi.org/10.1016/j.taml.2015.02.005.